

Seismic modeling in viscoelastic media

José M. Carcione*

ABSTRACT

Anelasticity is usually caused by a large number of physical mechanisms which can be modeled by different microstructural theories. A general way to take all these mechanisms into account is to use a phenomenologic model. Such a model which is consistent with the properties of anelastic media can be represented mechanically by a combination of springs and dashpots. A suitable system can be constructed by the parallel connection of several standard linear elements and is referred to as the general standard linear solid rheology. Two relaxation functions that describe the dilatational and shear dissipation mechanisms of the medium are needed. This model properly describes the short and long term behaviors of materials with memory and is the basis for describing viscoelastic wave propagation.

This work presents two-dimensional (2-D) and three-dimensional (3-D) forward modeling in linear viscoelastic media. The theory implements Boltzmann's superposition principle based on a spectrum of relaxation mechanisms in the time-domain equation of motion by the introduction of the memory variables. The algorithm uses a polynomial interpolation of the evolution operator for time integration and the Four-

ier pseudospectral method for computation of the spatial derivatives. This scheme has spectral accuracy for band-limited functions with no temporal or spatial dispersion, a very important fact in anelastic wave propagation.

Examples are given of how to pose typical problems of viscoelastic forward modeling for geophysical problems in two and three dimensions. A model separating an elastic medium of a viscoelastic medium with similar elastic moduli but different attenuations shows that the interface generates appreciable reflected energy. A second example computes the response of a single interface in the presence of highly dissipative sandstone lenses, properly simulating the anelasticity of direct and converted P- and S-waves. A common-shot reflection survey over a gas cap reservoir indicates that attenuation significantly affects the bright spot response. 3-D viscoelastic modeling requires twice the memory storage of 3-D viscoacoustic modeling when one dissipation mechanism is used for each wave mode. Simulation in a 3-D homogeneous viscoelastic medium shows how the anelastic characteristics of the different modes can be controlled independently. The result of this simulation is compared to the analytical solution indicating sufficient accuracy for many applications.

INTRODUCTION

Wave motion in real media is in many respects different from motion in an ideal elastic solid. Effects such as wave attenuation and dispersion significantly affect the amplitude and traveltimes of the wavefield. One of the first attempts to model anelastic waves with grid methods was carried out by Carcione et al. (1988a, b) where they introduce the time-domain viscoacoustic wave equation and present some geophysical applications in 2-D media. In this work, I approach

the description of a real medium by modeling the anelastic effects with a two-dimensional (2-D) and a three-dimensional (3-D) linear viscoelastic rheology.

In a linear viscoelastic solid, the stress tensor can be expressed as the time convolution of a time-dependent relaxation matrix with the time derivative of the strain tensor. The time dependence of the relaxation components is governed by material relaxation times. Each physical dissipation mechanism is described by pairs of relaxation times that give a minimum in the quality factor versus frequency,

Presented at the 59th Annual International Meeting, Society of Exploration Geophysicists. Manuscript received by the Editor October 2, 1991; revised manuscript received June 18, 1992.

*Osservatorio Geofisico Sperimentale, P.O. Box 2011, 34016 Trieste, Italy, and Geophysical Institute, Hamburg University, Bundesstrasse 55, 2000 Hamburg 13, Germany.

© 1993 Society of Exploration Geophysicists. All rights reserved.

with infinite values at the low- and high-frequency limits. A combination of several relaxation mechanisms can model any quality factor function versus frequency where the fitting parameters are the relaxation times.

The theory, developed in Carcione et al. (1988c), circumvents the convolutional relation between the stress and strain tensors by the introduction of the memory variables. In the 3-D case, the resulting wave equation is solved for the displacement field, one memory variable for each dissipation mechanism related to the dilatational wave, and five memory variables for each mechanism related to the shear wave. In the 2-D case, two memory variables are used for each shear relaxation mechanism. The problem is solved in the time domain by a new time integration method based on an optimum polynomial interpolation of the evolution operator (Tal-Ezer et al., 1990). This method is especially designed to solve wave propagation in linear viscoelastic media and greatly improves the spectral technique used in Carcione et al. (1988c). The spatial derivative terms are computed by means of the Fourier pseudospectral method. Similar approaches based on finite difference in time (a Taylor expansion of the evolution operator) and space were given in Day and Minster (1984), and in Emmerich and Korn (1987) for the viscoacoustic wave equation.

In the earth, there are cases where the impedance contrast is very weak but the contrast in attenuation is significant, i.e., if one of the materials is very unconsolidated or has fluid-filled pores. To simulate this situation, I present an example of waves impinging on a plane interface separating an elastic material of a viscoelastic medium with similar elastic moduli and density but different quality factors (Q interface). A second example displays a common shot time section in a medium that includes highly anelastic lens-shaped bodies. Then, I compute the seismic response to a single shot of a complex structure containing a gas cap in an anticlinal fold, a typical trap in exploration geophysics. Finally, I consider examples of wave simulation in 3-D homogeneous and inhomogeneous structures. The algorithm is tested against the analytical solution, which is based on a 3-D viscoelastic Green's function derived from the correspondence principle.

EQUATION OF MOTION

The time-domain equation of motion of an $n - D$ viscoelastic medium is formed with the following equations (Carcione, 1987; Carcione et al., 1988c):

- 1) The linearized equations of momentum conservation:

$$\rho \ddot{u}_i = \frac{\partial \sigma_{ij}}{\partial x_j} + \rho f_i, \quad i = 1, \dots, n,$$

where $\mathbf{x} = (x_1, x_2, x_3) \equiv (x, y, z)$ is the position vector, $\sigma_{ij}(\mathbf{x}, t)$ are the stress components, $u_i(\mathbf{x}, t)$ are the displacements, $\rho(\mathbf{x})$ denotes the density, and $f_i(\mathbf{x}, t)$ are the body forces, t being the time variable. Repeated indices imply summation and a dot above a variable indicates time differentiation.

- 2) The stress-strain relations:

$$\begin{aligned} \sigma_{xx} = & (\lambda_u + 2\mu_u) \frac{\partial u_x}{\partial x} + \lambda_u \left(\frac{\partial u_y}{\partial y} + \frac{\partial u_z}{\partial z} \right) \\ & + \left(\lambda_r + \frac{2}{n} \mu_r \right) \sum_{\ell=1}^{L_1} e_{1\ell} + 2\mu_r \sum_{\ell=1}^{L_2} e_{11\ell}, \end{aligned} \quad (2a)$$

$$\begin{aligned} \sigma_{yy} = & (\lambda_u + 2\mu_u) \frac{\partial u_y}{\partial y} + \lambda_u \left(\frac{\partial u_x}{\partial x} + \frac{\partial u_z}{\partial z} \right) \\ & + \left(\lambda_r + \frac{2}{n} \mu_r \right) \sum_{\ell=1}^{L_1} e_{1\ell} + 2\mu_r \sum_{\ell=1}^{L_2} e_{22\ell}, \end{aligned} \quad (2b)$$

$$\begin{aligned} \sigma_{zz} = & (\lambda_u + 2\mu_u) \frac{\partial u_z}{\partial z} + \lambda_u \left(\frac{\partial u_x}{\partial x} + \frac{\partial u_y}{\partial y} \right) \\ & + (\lambda_r + 2\mu_r) \sum_{\ell=1}^{L_1} e_{1\ell} \\ & - \frac{2}{n} \mu_r \sum_{\ell=1}^{L_2} (e_{11\ell} + e_{22\ell}), \end{aligned} \quad (2c)$$

$$\sigma_{xy} = \mu_u \left(\frac{\partial u_x}{\partial y} + \frac{\partial u_y}{\partial x} \right) + \mu_r \sum_{\ell=1}^{L_2} e_{12\ell}, \quad (2d)$$

$$\sigma_{xz} = \mu_u \left(\frac{\partial u_x}{\partial z} + \frac{\partial u_z}{\partial x} \right) + \mu_r \sum_{\ell=1}^{L_2} e_{13\ell}, \quad (2e)$$

$$\sigma_{yz} = \mu_u \left(\frac{\partial u_y}{\partial z} + \frac{\partial u_z}{\partial y} \right) + \mu_r \sum_{\ell=1}^{L_2} e_{23\ell}, \quad (2f)$$

where

$$\lambda_u = \left(\lambda_r + \frac{2}{n} \mu_r \right) M_{u1} - \frac{2}{n} \mu_r M_{u2}, \quad (3a)$$

and

$$\mu_u = \mu_r M_{u2}, \quad (3b)$$

are the unrelaxed or high-frequency Lamé constants, with λ_r and μ_r the relaxed or low-frequency Lamé constants. M_{uv} , $v = 1, 2$ are relaxation functions evaluated at $t = 0$, with $v = 1$, the dilatational mode, and $v = 2$, the shear mode. For the general standard linear solid rheology, they are given by

$$M_{uv} = 1 - \sum_{\ell=1}^{L_v} \left(1 - \frac{\tau_{\varepsilon\ell}^{(v)}}{\tau_{\sigma\ell}^{(v)}} \right), \quad v = 1, 2, \quad (4)$$

with $\tau_{\sigma\ell}^{(v)}$ and $\tau_{\varepsilon\ell}^{(v)}$ material relaxation times. The quantities $e_{1\ell}(\mathbf{x}, t)$ are memory variables related to the L_1 mechanisms which describe the anelastic characteristics of the dilatational wave, and $e_{11\ell}(\mathbf{x}, t)$, $e_{22\ell}(\mathbf{x}, t)$, $e_{12\ell}(\mathbf{x}, t)$, $e_{13\ell}(\mathbf{x}, t)$, and $e_{23\ell}(\mathbf{x}, t)$ are memory variables related to the L_2 mechanisms of the quasi-shear wave.

3) The memory variable first-order equations in time:

$$\dot{e}_{1\ell} = \Theta \phi_{1\ell} - \frac{e_{1\ell}}{\tau_{\sigma\ell}^{(1)}}, \quad \ell = 1, \dots, L_1, \quad (5a)$$

$$\dot{e}_{11\ell} = \left(\frac{\partial u_x}{\partial x} - \frac{\Theta}{n} \right) \phi_{2\ell} - \frac{e_{11\ell}}{\tau_{\sigma\ell}^{(2)}}, \quad \ell = 1, \dots, L_2, \quad (5b)$$

$$\dot{e}_{22\ell} = \left(\frac{\partial u_y}{\partial y} - \frac{\Theta}{n} \right) \phi_{2\ell} - \frac{e_{22\ell}}{\tau_{\sigma\ell}^{(2)}}, \quad \ell = 1, \dots, L_2, \quad (5c)$$

$$\dot{e}_{12\ell} = \left(\frac{\partial u_x}{\partial y} + \frac{\partial u_y}{\partial x} \right) \phi_{2\ell} - \frac{e_{12\ell}}{\tau_{\sigma\ell}^{(2)}}, \quad \ell = 1, \dots, L_2, \quad (5d)$$

$$\dot{e}_{13\ell} = \left(\frac{\partial u_x}{\partial z} + \frac{\partial u_z}{\partial x} \right) \phi_{2\ell} - \frac{e_{13\ell}}{\tau_{\sigma\ell}^{(2)}}, \quad \ell = 1, \dots, L_2, \quad (5e)$$

$$\dot{e}_{23\ell} = \left(\frac{\partial u_y}{\partial z} + \frac{\partial u_z}{\partial y} \right) \phi_{2\ell} - \frac{e_{23\ell}}{\tau_{\sigma\ell}^{(2)}}, \quad \ell = 1, \dots, L_2, \quad (5f)$$

where

$$\Theta = \frac{\partial u_x}{\partial x} + \frac{\partial u_y}{\partial y} + \frac{\partial u_z}{\partial z} \quad (6)$$

is the dilatation field, and

$$\phi_{v\ell} = \frac{1}{\tau_{\sigma\ell}^{(v)}} \left(1 - \frac{\tau_{\epsilon\ell}^{(v)}}{\tau_{\sigma\ell}^{(v)}} \right), \quad v = 1, 2, \quad (7)$$

are the response function components evaluated at $t = 0$. The low-frequency or elastic limit is obtained when $\tau_{\epsilon\ell}^{(v)} \rightarrow \tau_{\sigma\ell}^{(v)}$, $\forall \ell$; thus, $M_{uv} \rightarrow 1$ and $\phi_{v\ell} \rightarrow 0$, and the memory variables vanish. On the other hand, at the high-frequency limit the system also behaves elastically, corresponding to the instantaneous response. As can be seen from the stress-strain equations, the mean stress depends only on the parameters and memory variables with index $v = 1$ which involve dilatational dissipation mechanisms. Similarly, the deviatoric stress components depend on the parameters and memory variables with index $v = 2$, involving shear mechanisms. The 3-D case is obtained with $n = 3$, the 2-D case with $n = 2$ and, say, $\partial/\partial y [\cdot] = 0$, $\sigma_{yy} = \sigma_{xy} = \sigma_{zy} = 0$, and $e_{22\ell} = e_{12\ell} = e_{23\ell} = 0$. The elastic case is obtained by taking $\tau_{\epsilon\ell} = \tau_{\sigma\ell}$, $\forall \ell$ (low-frequency limit), or by zeroing the memory variables and taking the unrelaxed Lamé constants as the elastic Lamé constants (high-frequency limit). Viscoacoustic wave propagation is simply obtained by setting $\mu_r = 0$; the resulting equation can be written in terms of the dila-

tation 0, or in terms of the pressure $p = -\sigma_{xx} = -\sigma_{yy} = -\sigma_{zz}$. The system of equations (1), (2a, f) and (5a, f) is solved for the displacement field and memory variables by using a new spectral algorithm as a time marching scheme (Tal-Ezer et al., 1990). To balance time integration and spatial accuracies, the spatial derivatives are computed by means of the Fourier pseudospectral method.

2-D WAVE PROPAGATION

Q interface

This example considers wave propagation across an interface separating media with different quality factors but similar elastic moduli. The left half-space is elastic and the right half-space is viscoelastic (see Figure 4). The viscoelastic medium has almost constant quality factors in the seismic exploration band, as can be seen in Figure 1 where the bulk (Q_k), compressional (Q_p), and shear (Q_s) quality factors are plotted. Relaxation times are $\tau_{\epsilon 1}^{(1)} = 0.0334$ s, $\tau_{\sigma 1}^{(1)} = 0.0303$ s, $\tau_{\epsilon 1}^{(2)} = 0.0352$ s, $\tau_{\sigma 1}^{(2)} = 0.0287$ s, $\tau_{\epsilon 2}^{(1)} = 0.0028$ s, $\tau_{\sigma 2}^{(1)} = 0.0025$ s, $\tau_{\epsilon 2}^{(2)} = 0.0029$ s, and $\tau_{\sigma 2}^{(2)} = 0.0024$ s. The group and phase velocities are displayed in Figure 2a and 2b for P- and S-waves, respectively; they indicate strong wave dispersion. Expressions for the quality factors and wave velocities in viscoelastic media can be found in Carcione et al. (1988c).

The compressional and shear-wave velocities of the elastic medium are chosen in such a way as to minimize the normal PP and SS reflection coefficients at the central frequency of the source (25 Hz) whose spectra is plotted in Figure 1 with a dotted line. As stated by the correspondence principle (Bland, 1960), the reflection and transmission coefficients for an interface in attenuating media may be obtained from their analogues in elastic media by merely substituting the elastic velocities for the complex anelastic velocities. Assuming constant density in the whole space, the normal incidence reflection coefficient simply becomes $R(x) = (V - x)/(V + x)$, where V is the P-wave (S-wave)

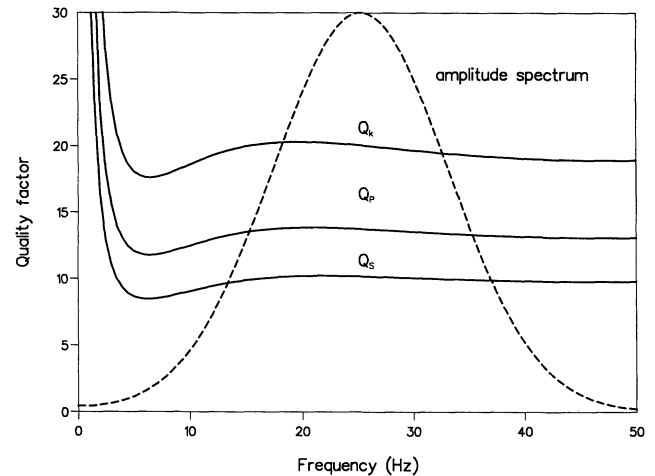


FIG. 1. P-wave, S-wave, and bulk quality factors for the viscoelastic medium of the Q interface. The dashed line represents the amplitude spectrum of the source.

complex velocity of the viscoelastic medium, and x is the unknown elastic velocity. Minimizing $R(x)$ gives the P - and S -wave elastic velocities $V_P = 3249$ m/s and $V_S = 2235$ m/s, respectively. Therefore, I obtain an almost Q interface where the elastic Q 's are infinite and the viscoelastic Q 's are represented in Figure 1. A different way to get such an interface is to choose as elastic velocities the phase velocities of the viscoelastic medium at the central frequency of the source. The two procedures are equivalent if $Q_P, Q_S \gg 1$. The viscoelastic reflection and transmission coefficients versus incidence angle for a compressional wave incident from the elastic medium at the central frequency of the source are represented in Figure 3. As can be seen, the values become significant at large angles.

The simulation uses a 165×165 mesh with grid spacing $D_x = D_z = 20$ m. The source, a Z -directional point force indicated by an arrow in Figure 4, is located in the elastic medium. Its time dependence is a Ricker wavelet. Snapshots at $t = 0.44$ s are shown in Figure 4a (u_x -component) and 4b (u_z -component). The strong attenuation in the anelastic medium is apparent. The inner wavefront (S -wave) is relatively more attenuated than the outer wavefront (P -wave), a

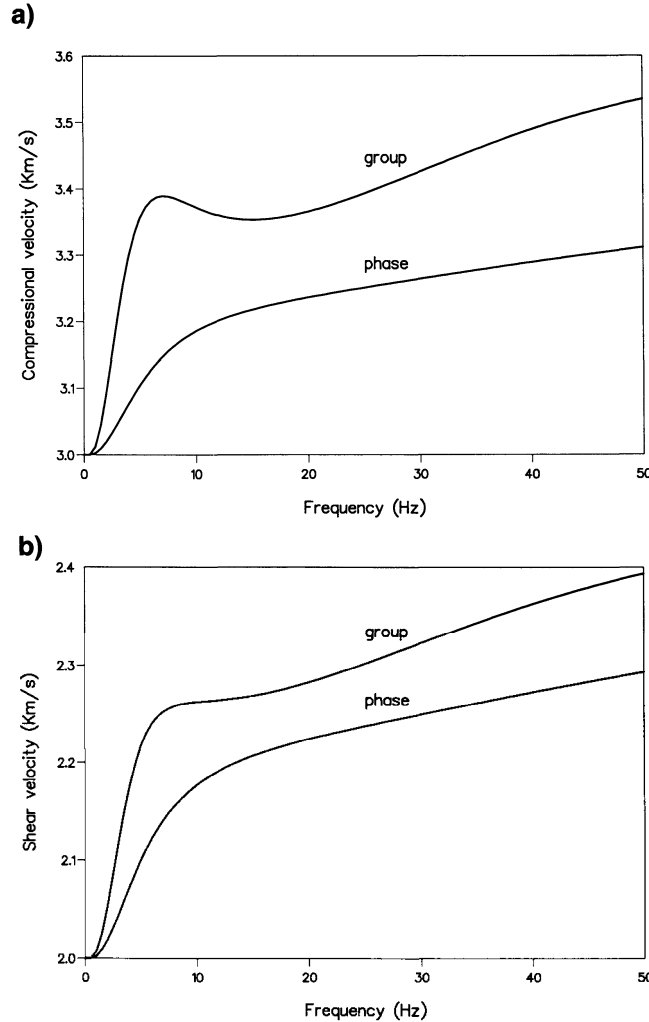


FIG. 2. Phase and group velocities for the viscoelastic half-space of the Q interface model, (a) P -waves, and (b) S -waves.

consequence of the lower S quality factor. Although I tried to avoid impedance contrasts at the central frequency, a reflected SS -wave can be clearly seen together with a PS -head wave and a PS -transmitted wave. It is clear that due to the particular choice of the elastic velocities there is a velocity inversion for low frequencies and the opposite effect for high frequencies. This phenomenon can only take place when at least one of the materials is anelastic.

Low Q inclusions model

The geologic model is shown in Figure 5. The perturbation is initiated by a vertical point source with a Ricker time history, and it is recorded at the top of the model. The material properties are indicated in Table 1. Relaxed moduli and relaxation times are chosen to give almost constant Q values and equal phase velocities at the central frequency of the source (20 Hz) in media 1, 2, and 3 (Q contrast only). Medium 4 is purely elastic. The numerical model uses a 105×105 grid with a spacing $D_x = D_z = 20$ m. To eliminate wraparound from the boundaries, absorbing strips are placed around the numerical mesh (Kosloff and Kosloff, 1986).

Figure 6 compares elastic and viscoelastic time sections, respectively, with (a) the u_x -component, and (b) the u_z -component. The elastic time sections are calculated by using as elastic velocities the relaxed velocities indicated in Table 1. The wavefield on the right side of the time sections is strongly attenuated due to the presence of the low Q inclusions, the shear wave being the more affected. These effects can be clearly seen in the PS , SS , and S direct events.

Anticlinal trap model

In this example, a common-shot seismogram of an inhomogeneous structure with a wide range of seismic velocities and quality factors is computed. The geologic model is

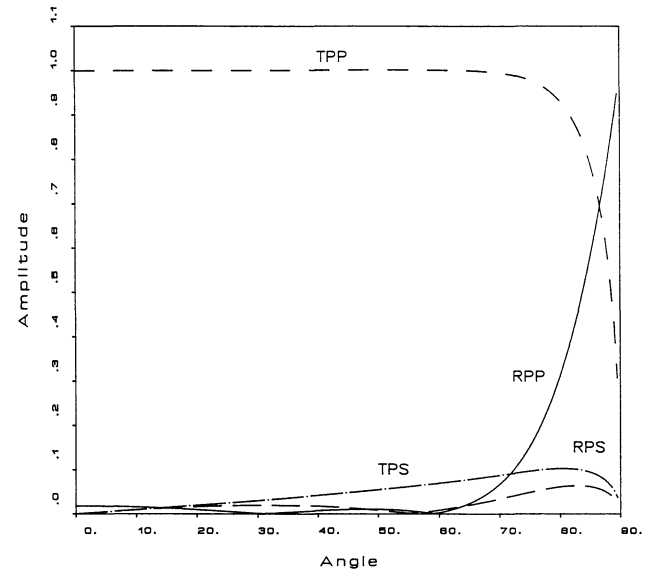


FIG. 3. Reflection and transmission coefficient at 25 Hz corresponding to the Q interface model for a P -wave incident from the elastic medium.

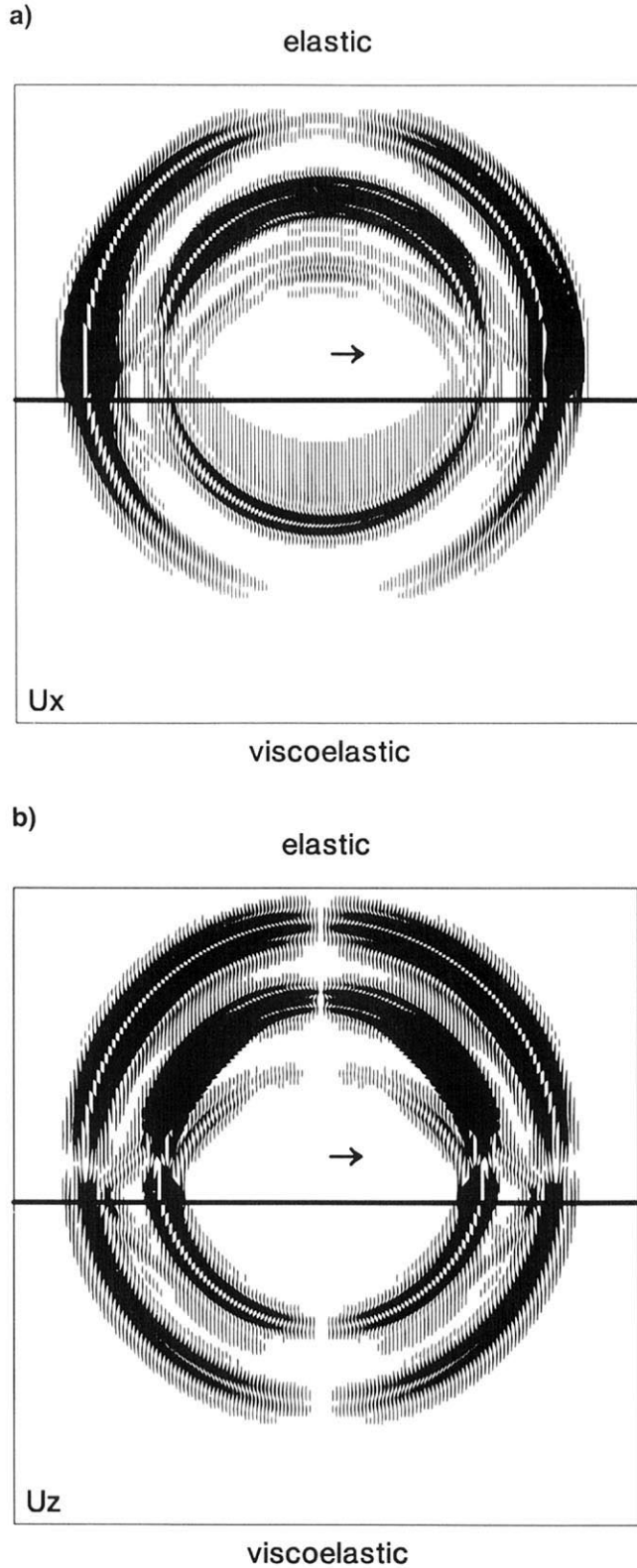


FIG. 4. Snapshots at $t = 0.44$ s for the Q interface model, where (a) is the u_x -component, and (b) the u_z -component.

represented in Figure 7. It is a typical hydrocarbon trap where the reservoir rock, a permeable sandstone, is saturated with gas in region 5, and with brine in region 6. The gas cap zone and the brine saturated sandstone are highly dissipative. The anticlinal fold is enclosed between impermeable shales represented by media 4 and 7. The material properties are indicated in Table 2 together with the relaxed velocities. The quality factors were chosen such that they have constant value around the dominant frequency of the wavelet (20 Hz).

Synthetic seismograms are calculated for a pressure source located in the weathering zone. The receivers are placed at the top of the model as indicated in Figure 7. The calculations use a grid size of $N_x = 221$ and $N_z = 221$, with horizontal and vertical grid spacings of $D_x = D_z = 20$ m. To prevent wavefield wraparound, I use an absorbing region of 18 points surrounding the numerical mesh. For comparison, the elastic response is also computed. The relaxed velocities given in Table 2 are taken as elastic velocities. The seismic responses are shown in Figure 8, where (a) indicates elastic, and (b) and (c) viscoelastic cases. Figure 8c displays the same data given in (b) with an additional uniform gain (factor three).

The bright spot event is a combination of reflections from the upper and lower interfaces of the anticline and gas-brine contact. Since these reflections are very close to each other, the characteristics of the bright spot are significantly altered by the anelastic effects. In particular, the reflection from the bottom of the anticline has practically disappeared due to the strong attenuation inside the gas cap region.

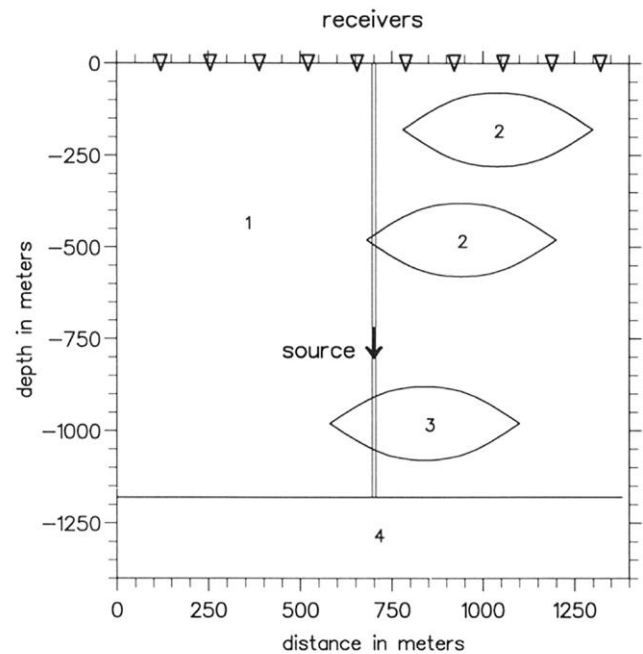
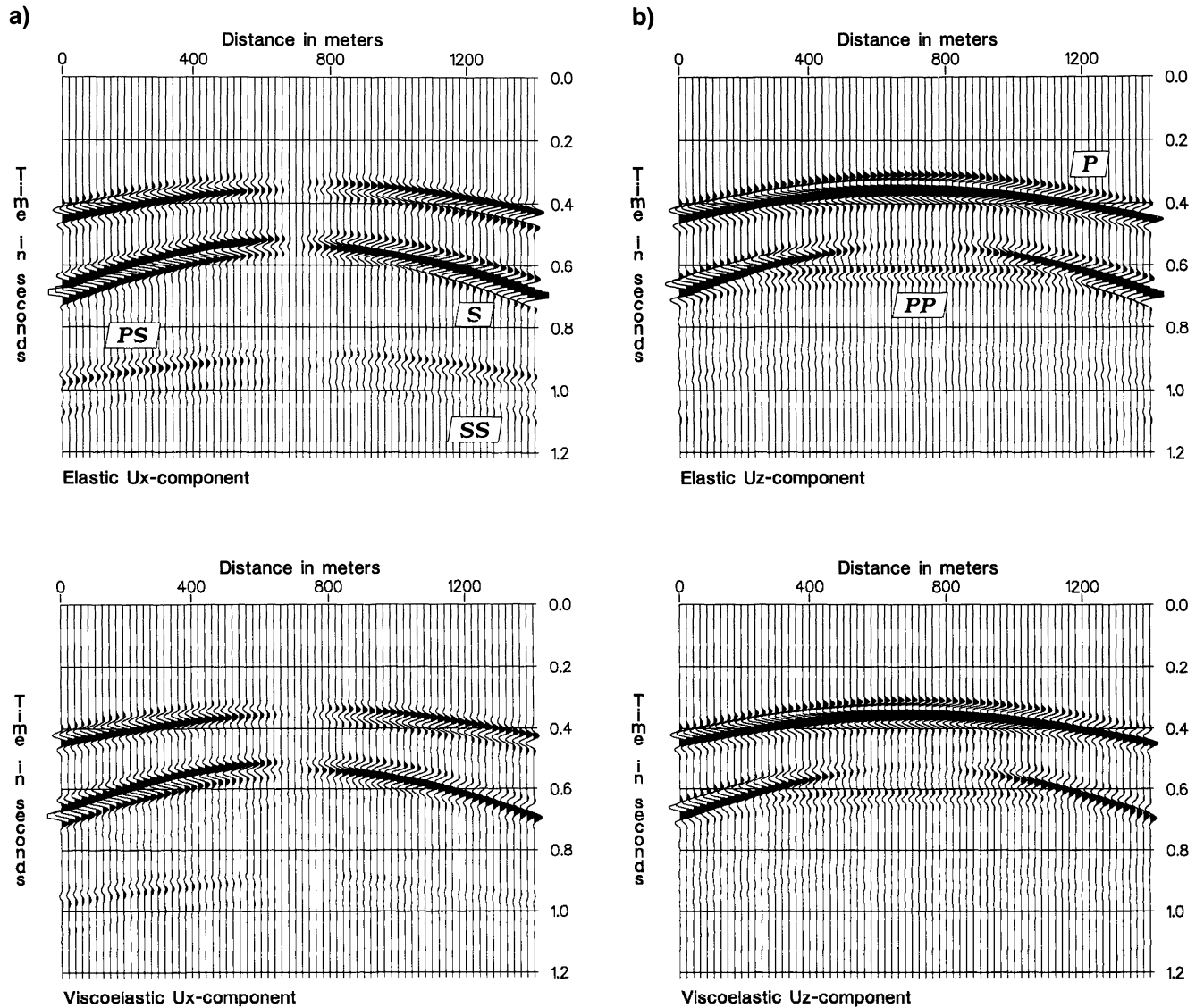


FIG. 5. Configuration and structure for the low Q inclusions model. The numbers indicate the media whose properties are given in Table 1.

Table 1. Material properties of low Q inclusions model.

Medium	0 Hz	V_P (m/s) 20 Hz	∞ Hz	0 Hz	V_S (m/s) 20 Hz	∞ Hz	ρ (Kg/m ³)	Q_k	Q_P	Q_S
1	2785	2800	2813	1685	1700	1710	2000	200	145	100
2	2620	2800	2974	1535	1700	1849	2000	20	15	10
3	2720	2800	2882	1630	1700	1773	2000	40	30	20
4	4000	4000	4000	2500	2500	2500	2000	∞	∞	∞

FIG. 6. Comparison of elastic and viscoelastic synthetic seismograms for the low Q inclusions model (a) is the u_x -component, and (b) the u_z -component.

3-D WAVE PROPAGATION

Practical applications of 3-D forward modeling require large quantities of CPU memory, typically tens of megawords of storage, a size that exceeds the central memory of most computer systems. Specific details about the computer optimization and implementation of 3-D viscoelastic codes on vector and parallel computers are similar to those given in Reshef et al. (1988a, b) for elastic problems. As here, they use the Fourier method to calculate the spatial derivatives but a second-order finite-difference scheme to match the solution in time. This results in an unbalanced scheme with infinite spatial accuracy but only second-order temporal accuracy. Instead, the present algorithm uses spectral methods both in time and space, avoiding in this way any numerical dispersion and achieving machine accuracy efficiently. The Fourier method is based on the prime factor fast-Fourier transform (FFT) (Temperton, 1988) where the length of each FFT is the product of odd prime numbers. Calculation with Nyquist wavenumbers is avoided.

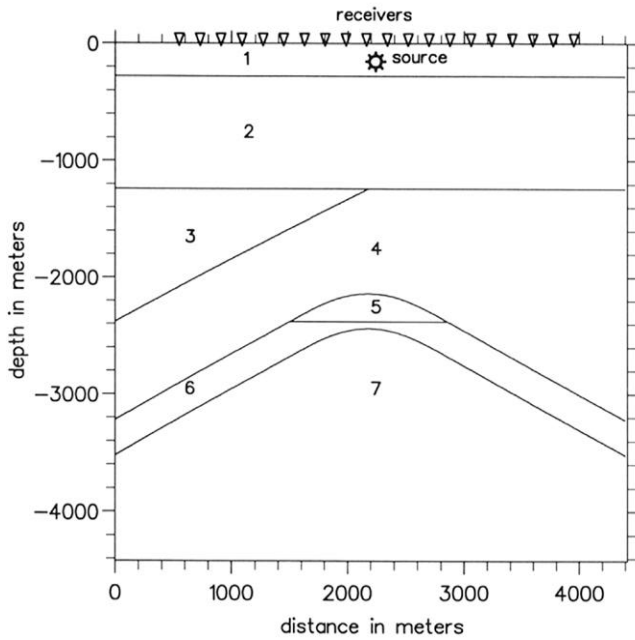


FIG. 7. Configuration and structure for the anticlinal trap model. The numbers indicate the media whose properties are given in Table 2.

Table 2. Material properties anticlinal trap model.

Medium	V_p (m/s)	V_s (m/s)	ρ (Kg/m ³)	Q_k	Q_p	Q_s
1	2600	1500	2400	80	50	30
2	3200	1850	2530	100	80	60
3	4000	2300	2670	120	100	80
4	5200	3000	2850	250	180	120
5	3650	2100	2610	30	17	10
6	4300	2480	2720	60	45	30
7	6000	3460	2960	300	280	250

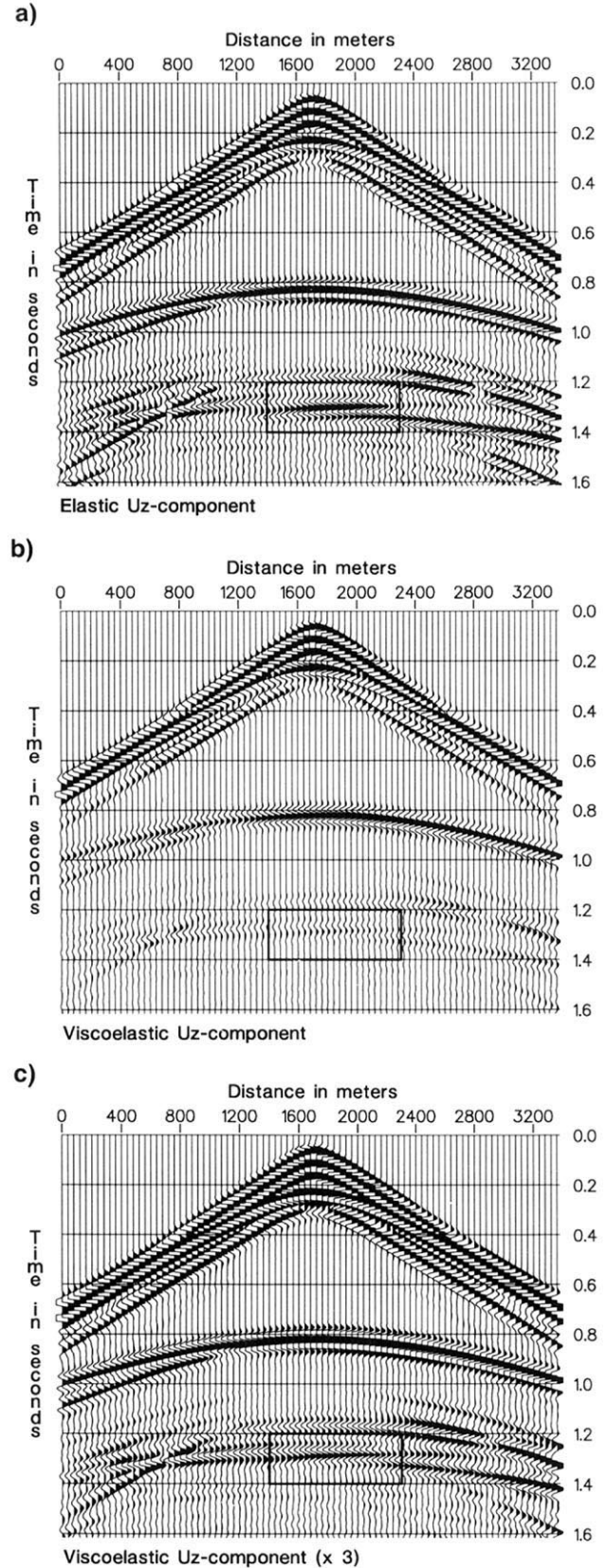


FIG. 8. The u_z -component synthetic seismograms of the anticlinal trap model, (a) is the elastic, (b) the viscoelastic, and (c) the viscoelastic with an additional uniform gain (factor three).

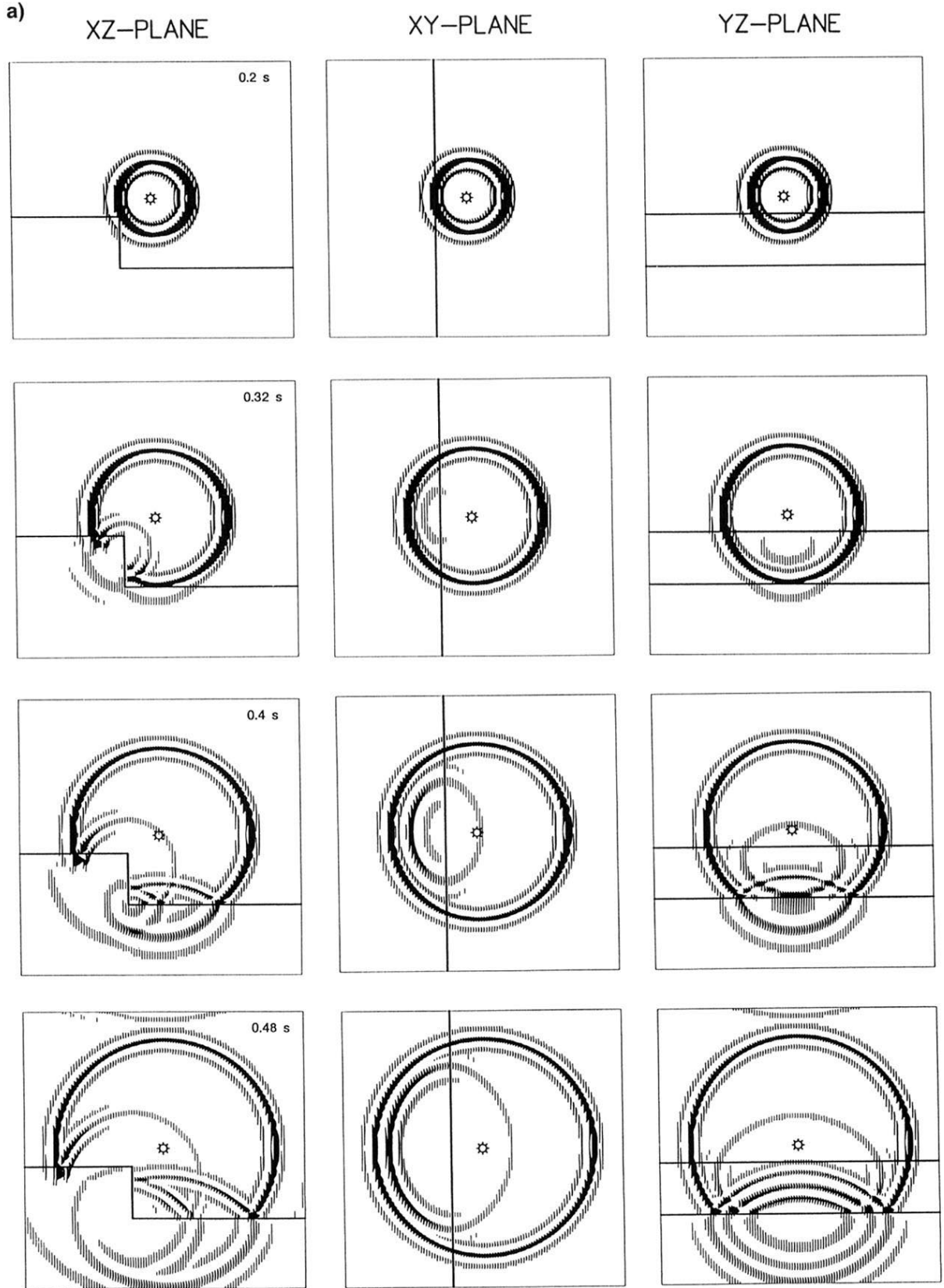


FIG. 9. Snapshots of the step structure at several propagation times on three mutually perpendicular planes passing through the source, where (a) acoustic and (b) viscoacoustic. The snapshots are scaled with respect to the acoustic snapshot at 0.2 s in the XZ -plane.

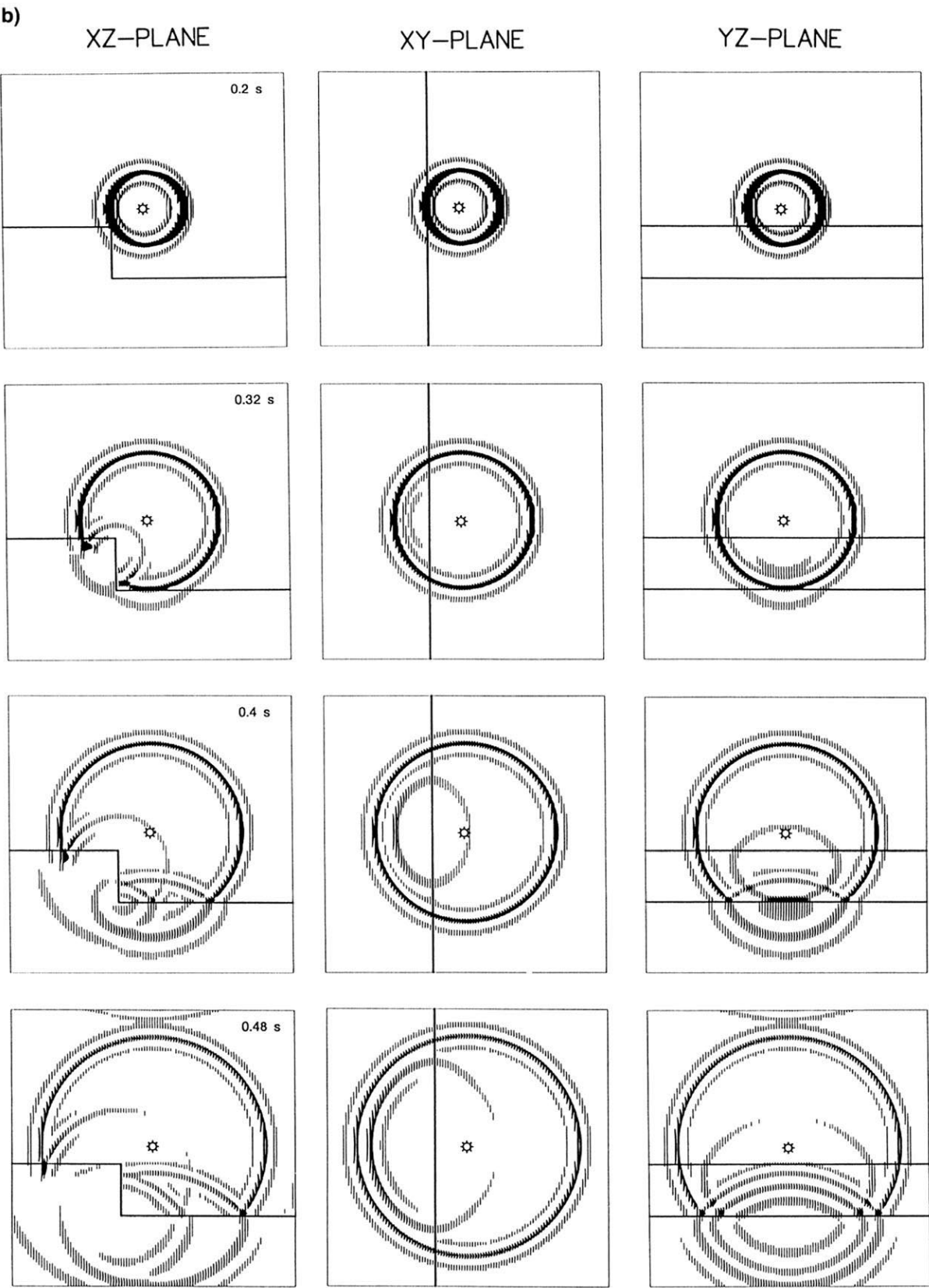
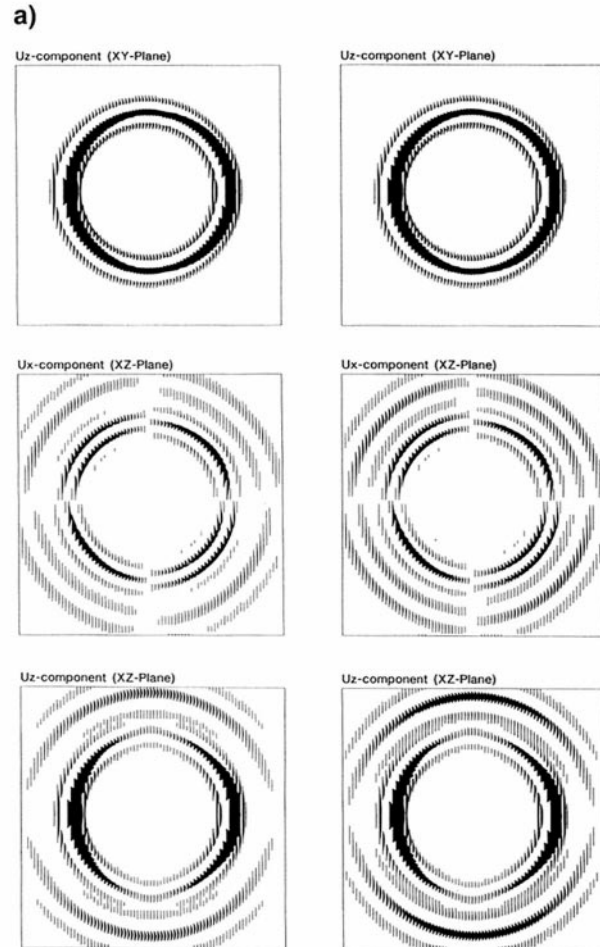


FIG. 9. (continued)

Implementation of the algorithm for the viscoelastic case needs three times the number of variables at each grid point, where the variables are: three displacements, three particle velocities, plus $L_1 + 5L_2$ memory variables. Moreover, the algorithm uses six additional arrays for temporal storage, and arrays for the material parameters $3 + 2(L_1 + L_2)$, i.e., relaxed Lamé constants, density, and pairs of relaxation times. Therefore, the total number of arrays is then $M = 27 + 5L_1 + 17L_2$, and total memory requirements are given by $MN_XN_YN_Z$ million words. The viscoacoustic code uses $2 + L_1$ unknown variables, three additional arrays for storage, and $2 + 2L_1$ material parameters, giving $M = 11 + 5L_1$ arrays. The tests were done on an Apollo IO 000 computer system with a vector facility.

Step structure

Here I compute the response of a 3-D step, actually a 2 112-D medium since the step is in the XZ-plane with no variation of material properties in the Y-direction. The rheology is viscoacoustic with the upper medium having a single dissipation mechanism with relaxation times $\tau_e = 0.00678$ s and $\tau_\sigma = 0.00645$ s. They give a quality factor of $Q \approx 40$ around the central frequency of the source, $f_0 = 25$ Hz. The relaxed wave velocity of the upper medium is 2000 m/s. The lower medium is purely elastic with relaxed velocity 3500 m/s. The density is constant throughout the model space.



The grid size used is $108 \times 108 \times 108$ with a spacing of 20 m in every direction. The source is located at grid point (54, 54, 54). Viscoacoustic and acoustic snapshots for several times are displayed in Figures 9a and 9b, respectively. The snapshots are scaled relative to the acoustic snapshot at 0.2 s in the XZ-plane. The attenuation is evident at large propagation times.

Homogenous viscoelastic medium

In this idealized numerical experiment, only the P-wave dissipates energy. The relaxation times are chosen such that the S-wave has elastic behavior. This holds when $\tau_{\epsilon\ell}^{(2)} = \tau_{\sigma\ell}^{(2)}$, $\forall \ell$. The attenuation of the P-wave is due to a single dissipation mechanism with relaxation times $\tau_e^{(1)} = 0.00678$ s and $\tau_\sigma^{(1)} = 0.00570$ s, which give the quality factors $Q_k \approx 12$ and $Q_p \approx 20$ at the central frequency of the source, 25 Hz for this problem. The relaxed wave velocities are $V_p = 3000$ m/s and $V_s = 2000$ m/s.

The parameters of the numerical mesh are $N_X = N_Y = N_Z = 81$, with a 20 m grid spacing in each direction. The initial motion is a Z-directional point source located at the center of the 3-D region. Figure 10a compares elastic and viscoelastic snapshots on planes passing through the source position. Propagation time is 0.3 s. By symmetry, u_y (YZ-plane) = u_x (XZ-plane) and u_z (YZ-plane) = u_z (XZ-plane), while u_y (XZ-plane), u_x (YZ-plane), u_x (XY-plane), and u_y (XY-plane) vanish. In the XY-plane, there is mainly shear motion. As can be seen, the P-wave (outer wavefront) has attenuated and dispersed while the S-wave has not (inner wavefront).

The numerical solution at the vertical axis is compared to the 3-D analytical solution in Figure 10b. The dotted line represents the elastic numerical solution. The comparison is at 400 m from the source position. The analytical solution is obtained by applying the correspondence principle to the frequency-domain elastic analytical solution (e.g., Pilant, 1979, p. 67), and then performing an inverse Fourier transform back to the time domain. Only the u_z -component is different from zero. As the figure shows, the comparison is

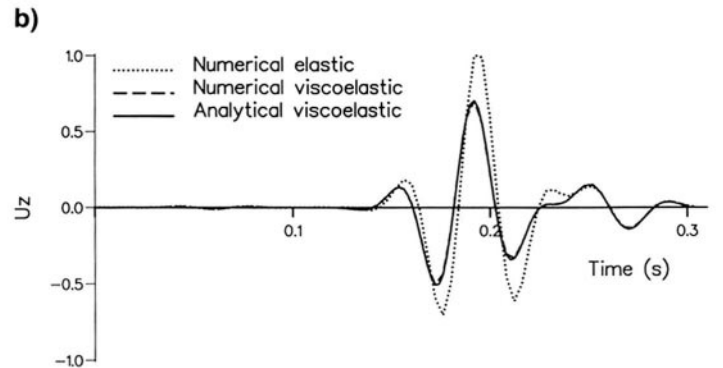


FIG. 10. (a) Elastic (left) and viscoelastic (right) in a 3-D homogeneous viscoelastic medium. Attenuation only affects the P-wave. (b) Comparison between the numerical and analytical solution at the vertical axis. The dotted line represents the elastic numerical solution.

excellent. The response is mainly P-motion which contributes with a first-order term proportional to z^{-1} . This pulse has been dissipated and shows a time lead with respect to the elastic solution. There are also contributions from higher order terms due to P- and S-motions. These are diffracted or near-field terms that should be negligible at long propagation distances. However, they are still important in this case, and can be seen between 0.2 s and 0.3 s. In fact, the tail of the response in Figure 10b corresponds to an S-wave since it has not been affected by anelasticity.

CONCLUSIONS

Most applications of seismic forward modeling assume that the subsurface is an acoustic medium, and only in limited cases is an elastic rheology considered. When the aim is to model real geologic structures, for instance hydrocarbon reservoirs, these assumptions can hardly be justified since effects like attenuation and wave dispersion play an important role in the position and amplitude of the seismic events.

The present forward modeling scheme simulates the response of linear isotropic-anelastic media by using a phenomenological model based on the general standard linear solid rheology. The model embodies most of the dissipation mechanisms present in real rocks, in particular those that show relaxation behavior. The relaxation times are the parameters to model a realistic frequency-dependent quality factor and wave velocity.

The examples show how to deal with viscoelastic forward modeling in two and three dimensions. The first example computes the response of an interface separating regions of different attenuation characteristics. This system is used in the next example to model sandstone lenses with high dissipation. The modeling accurately describes the attenuation and dispersion of direct and converted P- and S-waves. Simulation of a gas cap reservoir indicates that the combination of interface geometry and the effects of anelasticity on P- and S-waves significantly alter the seismic response, in particular when the region to model is smaller or comparable to the source wavelength. The anelastic characteristics of P- and S-waves can be controlled independently by an appropriate choice of the relaxation times. The last 3-D example shows how one mode can be kept elastic. This fact is shown by comparison of elastic and viscoelastic snapshots and

verification with the analytical solution. The excellent matching between numerical and analytical solutions leads us to expect that the algorithm will produce accurate results for more complex problems.

Three-dimensional simulations in viscoelastic media require large quantities of storage, but wavefields for meaningful models can be computed even for relatively small computer systems. Today, realistic 3-D models require a vector and parallel supercomputer. In particular, the FFT routine is easily vectorizable and calculation at several groups of depth planes can be parallelized.

ACKNOWLEDGMENTS

This work was supported in part by the Commission of the European Communities under project EOS-1 (Exploration Oriented Seismic Modeling and Inversion), Contract N. JOUF-0033, part of the GEOSCIENCE project within the framework of the JOULE R & D Programme (Section 3.1.1.b).

REFERENCES

- Bland, D., 1960, The theory of linear viscoelasticity: Pergamon Press Ltd.
- Carcione, J. M., 1987, Wave propagation simulation in real media: PhD thesis, Tel-Aviv Univ.
- Carcione, J. M., Kosloff, D., and Kosloff, R., 1988a, Wave propagation simulation in a linear viscoacoustic medium: *Geophys. J. Roy. Astr. Soc.*, 93, 393-407.
- , 1988b, Viscoacoustic wave propagation simulation in the earth: *Geophysics*, 53, 769-777.
- , 1988c, Wave propagation simulation in a linear viscoelastic medium: *Geophys. J. Roy. Astr. Soc.*, 95, 597-611.
- Day, S. M., and Minster, J. B., 1984, Numerical simulation of attenuated wavefields using a Padé approximant method: *Geophys. J. Roy. Astr. Soc.*, 78, 105-118.
- Emmerich, H., and Korn, M., 1987, Incorporation of attenuation into time-domain computations of seismic wavefields: *Geophysics*, 52, 1252-1264.
- Kosloff, R., and Kosloff, D., 1986, Absorbing boundaries for wave propagation problems: *J. Comp. Phys.*, 63, 363-376.
- Pilant, W. L., 1979, Elastic waves in the earth: North-Holland Amsterdam.
- Reshef, M., Kosloff, D., Edwards, M., and Hsiung, C., 1988a, Three-dimensional elastic modeling by the Fourier method: *Geophysics*, 53, 1184-1193.
- , 1988b, Three-dimensional acoustic modeling by the Fourier method: *Geophysics*, 53, 1175-1183.
- Tal-Ezer, H., Carcione, J. M., and Kosloff, D., 1990, An accurate and efficient scheme for wave propagation in a linear viscoelastic medium: *Geophysics*, 55, 1366-1379.
- Temperton, C., 1988, Implementation of a prime factor FFT algorithm on CRAY-1: *Parallel Computing*, 6, 99-108.